Journal of Instrumentation

PAPER

Single-line multi-voltage threshold method for scintillation detectors

To cite this article: Hyeyeun Chu *et al* 2023 *JINST* **18** P06021

Published by IOP Publishing for Sissa Medialab

Received: *April 13, 2023*
Accepted: *May 18, 2023*
Published: *June 21, 2023*

2023 JINST 18 P06021

Single-line multi-voltage threshold method for scintillation detectors

Hyeyeun Chu,[a,b,c] **Minseok Yi,**[a,b,c] **Hyeong Seok Shim**[a,b,c] **and Jae Sung Lee**[a,b,c,d,*]

[a] *Interdisciplinary program in Bioengineering, Seoul National University Graduate School, Seoul 03080, Republic of Korea*

[b] *Integrated Major in Innovative Medical Science, Seoul National University Graduate School, Seoul 03080, Republic of Korea*

[c] *Department of Nuclear Medicine, Seoul National University College of Medicine, 103 Daehak-ro, Jongno-gu, Seoul 03080, Republic of Korea*

[d] *Brightonix Imaging Inc., Seoul, Republic of Korea*

E-mail: jaes@snu.ac.kr

*Corresponding author.

 https://doi.org/10.1088/1748-0221/18/06/P06021

Abstract: The multiple thresholds used in multi-voltage threshold (MVT) method provide more detailed information about the pulse amplitude of the input analog pulses than the simple time-over-threshold (TOT) method, thus allowing for better energy estimation and pulse reconstruction capabilities. However, as the number of thresholds increases, the number of comparators and digital signal readout channels required for MVT also increases. This requirement owing to the increased number of thresholds is the main disadvantage of MVT implementation using field-programmable gate array (FPGA)-based time-to-digital converters (TDCs) because the FPGA resources required for TDC implementation are substantial and FPGAs have a limited number of input/output ports. Therefore, we propose a new single-line MVT method to improve the integrity of the FPGA-only data acquisition system without analog-to-digital converters by reducing the FPGA input channels required for the MVT method. The proposed method, which applies three different levels of thresholding, reduces the digital output signal line in the MVT by employing a 3-input XOR logic gate. The XOR gate integrates the output signals from the comparators and generates 1-bit line digital pulse train. We evaluated the energy performance of the proposed single-line MVT method using three different energy estimators. The energy estimates were compared with the ground truth energy calculated using domino-ring-sampler 4 (DRS4)-sampled analog pulses. The proposed method showed virtually equivalent energy resolution to that of DRS4-based pulse digitization method and better energy linearity than the conventional TOT method. Among the energy estimation methods used in single-line MVT, the *crossing-point triangular sum* method showed the best energy linearity. The proposed single-line MVT method will be useful when data acquisition systems without ADCs are implemented using FPGA-based TDCs. This is because the proposed method alleviates the problem of limited input ports and the numerous resources required for TDCs in FPGAs.

Keywords: Data acquisition circuits; Front-end electronics for detector readout; Gamma detectors (scintillators, CZT, HPGe, HgI etc)

Contents

1 Introduction

Scintillation detectors, consisting of scintillation crystals and photosensors, are widely used for the detection and measurement of ionizing radiation. A recent advance in scintillation detector technology is the widespread utilization of silicon photomultipliers (SiPMs), which have several advantages over conventional photomultiplier tubes [1–4]. Because SiPMs are insensitive to magnetic fields, they are most widely used in magnetic resonance imaging (MRI)-compatible positron emission tomography (PET) systems for simultaneous PET/MRI scans [5–11]. In addition, the compactness of the SiPM improves PET detector performance by increasing the light collection efficiency [12–14]. However, the high granularity of SiPMs due to their compact size has increased the number of output channels and the complexity of signal readout and data acquisition electronics. To overcome these problems, several analog signal multiplexing techniques have been proposed [15–22]. However, many advanced PET detectors, such as depth of interaction (DOI)-encoding detectors that use light distribution information [23, 24], require SiPM signal readout and recording with no or only moderate analog signal multiplexing.

Time-over-threshold (TOT) methods allow for the measurement of the energy information of scintillation detectors with a high level of integration and low power consumption [25]. Highly accurate energy measurements are possible using waveform digitizers or free-running analog-to-digital converters (ADCs) with high bandwidth and sampling rate [14, 26–30]. However, they are expensive, have high power consumption, and require relatively large space [31]. By contrast, the TOT technique estimates the energy (or charge) of a signal based on the signal pulse width, which is determined by certain reference threshold(s) and can be implemented simply using comparators and clock counters [32–35]. The accuracy of the TOT measurement can be improved by utilizing precise time-to-digital converters (TDCs) instead of simple clock counters. In addition, highly integrated TDCs can be implemented using field-programmable gate arrays (FPGAs) [36–39]. However, the simple TOT method using a single threshold suffers from inferior energy linearity compared with ADC-based measurements [17, 34, 40]. Therefore, several approaches have been proposed to overcome the limitations of the TOT method. These advanced approaches include the dynamic TOT method, which applies varying thresholds to the falling edge of the analog input pulse depending on the pulse height [41, 42], and the sawtooth-shaped threshold method, which obtains multiple digital pulses by applying a sawtooth-shaped threshold signal adaptively generated to the input pulse [43]. Another alternative is the widely used multi-voltage threshold (MVT) method, which applies two or more fixed thresholds to achieve better energy performance by utilizing multiple digital pulse trains with different widths [33, 44–46].

The multiple thresholds used in the MVT method provide more detailed information about the pulse amplitude and timing of the input analog pulses than the simple TOT method, thus allowing for better energy estimation and pulse reconstruction capabilities. However, as the number of thresholds increases, the number of comparators and digital signal readout channels required for MVT also increases. This requirement owing to the increased number of thresholds is the main disadvantage of MVT implementation using FPGA-based TDCs because the FPGA resources required for TDC implementation are substantial and FPGAs have the limited number of input/output ports.

Therefore, we propose a new single-line MVT method to improve the integrity of the FPGA-only data acquisition system without ADCs by reducing the FPGA input channels required for the MVT method. The proposed method, which applies three different levels of thresholding, reduces the digital output signal line in the MVT by employing a 3-input XOR logic gate. The XOR gate integrates the output signals from the comparators and generates 1-bit line digital pulse train. In the following sections, we describe how the proposed method was designed and how its characteristics were evaluated through experiments.

2 Materials and methods

2.1 Single-line MVT

The key concept of the single-line MVT method is to integrate digital pulses from each threshold into a single line using an XOR gate, as shown in figure 1. When an analog scintillation pulse passes through a comparator with a certain threshold, two timestamps are generated: one on the rising edge and the other on the falling edge. When three different thresholds were applied, three pairs of rising and falling edges were obtained. Applying a 3-input XOR gate to these three digital pulses produces a 1-bit line digital pulse train with six distinguished timestamps. To exploit the XOR gate, only an odd number of thresholds needs to be applied.

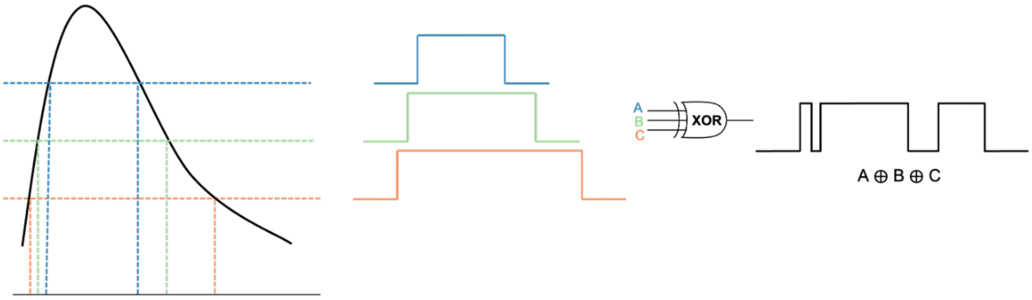

Figure 1. Schematic of proposed single-line multi-voltage threshold method implemented with a 3-input XOR gate.

Generally, the larger number of comparators used in the MVT method leads to better energy performance (e.g., energy resolution and linearity) but increases the complexity and cost of front-end and readout electronics [47]. Therefore, in this proof-of-concept study, only three comparators with different thresholds and a 3-input XOR gate were used for 1-bit line digital pulse generation.

2.2 Circuit implementation

Figure 2 shows the circuit diagram of the proposed single-line MVT method. The analog pulse from the photosensor (silicon photomultiplier) was amplified by a factor of 10 using a non-inverting amplifier (AD8000; Analog Devices) and passed through an RC low-pass filter. The low-pass filtered signal was fed to three comparators (ADCMP601; Analog Devices) with different thresholds, and the digital outputs of the comparators were merged into a single-line digital pulse using a 3-input XOR gate (NC7SZ386P6X; Onsemi).

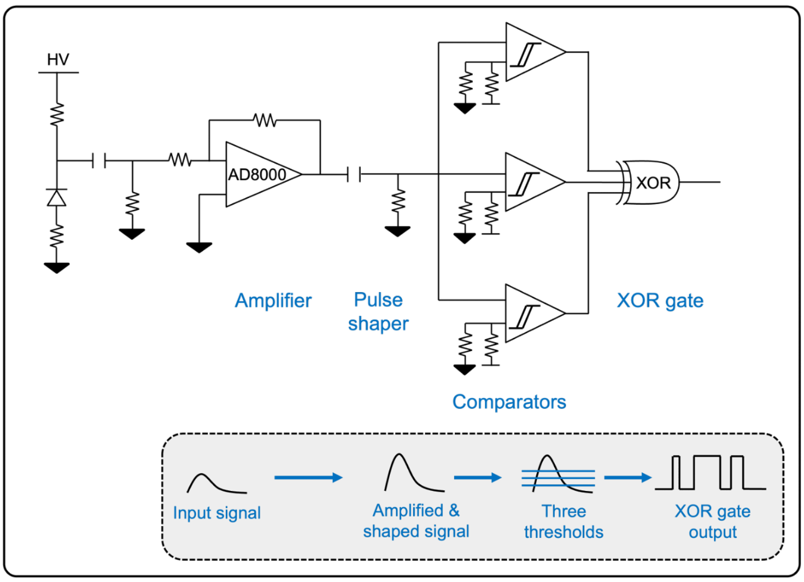

Figure 2. Circuit diagram for the single-line MVT method.

2023 JINST 18 P06021

2.3 Experimental setup

As shown in figure 3, analog scintillation pulses were obtained using an LYSO-SiPM detector in which a single 4×4 mm SiPM (ASD-EP-S-4; AdvanSiD; Trento, Italy) was coupled with a $3 \times 3 \times 20$ mm LYSO crystal by optical grease (BC-630 Silicone Grease; Saint Gobain Crystals, U.S.A.). A reference detector consisting of a photomultiplier tube and LYSO crystal was employed to generate a coincidence signal used as a trigger for a domino-ring-sampler 4 (DRS4)-based digitizer (DT5742B; CAEN, Italy), and a Na-22 source was attached to the reference detector. The analog scintillation pulses and single-line digital pulse trains from the MVT circuit were sampled at a sampling rate of 1 giga-samples/s. A total of 10,000 events, with 1,024 samples per pulse, were recorded.

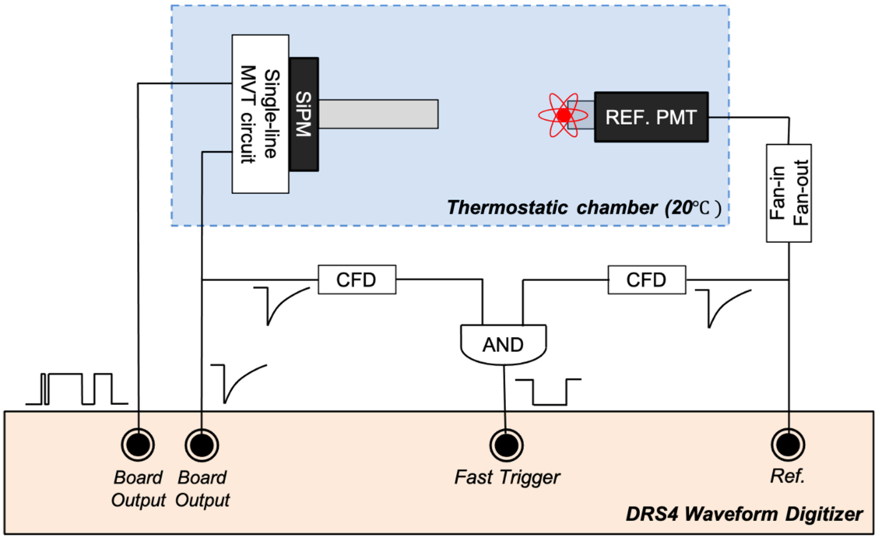

Figure 3. Experimental setup.

2.4 Energy estimator

In this technique, six discrete timestamps were derived from three different threshold voltages. We applied three different energy estimators, shown in figure 4, to estimate the energy of each pulse using six timestamps. The energy estimates were compared with the ground-truth energy calculated using DRS4-sampled analog pulses.

First, the *rectangular sum* was calculated by generating rectangles with threshold values and timestamps. Second, the *trapezoidal sum* was calculated by replacing the rectangles with trapezoids. Finally, the *crossing-point triangular sum* was calculated by adding the triangular area at the top of the pulse to the *trapezoidal sum*. The top vertex of the triangle is the crossing point of the two lines extrapolated using the two highest thresholds (th_2 and th_3) and their timestamps. Estimated energy (E) value from each method is expressed with threshold values and TOT values, which are interval between timestamps resulted in from thresholds. The estimated energy values of rectangular sum, trapezoidal sum, and crossing-point triangular sum are expressed as following

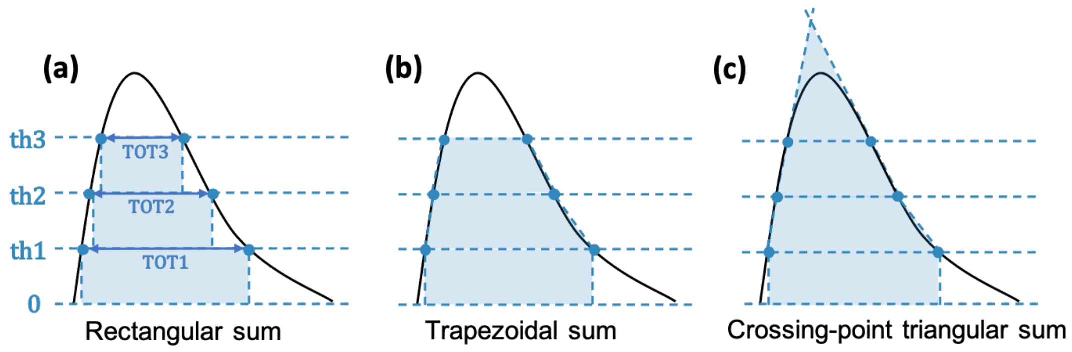

Figure 4. Three different numerical integration methods for energy estimation: (a) rectangular sum, (b) trapezoidal sum, and (c) crossing-point triangular sum.

equations from (2.1), (2.2), and (2.3), respectively.

$$E = \mathrm{th}_1 \cdot \mathrm{TOT}_1 + (\mathrm{th}_2 - \mathrm{th}_1) \cdot \mathrm{TOT}_2 + (\mathrm{th}_3 - \mathrm{th}_2) \cdot \mathrm{TOT}_3 \tag{2.1}$$

$$E = \frac{1}{2} \cdot (\mathrm{th}_1 + \mathrm{th}_2) \cdot \mathrm{TOT}_1 + \frac{1}{2} \cdot (\mathrm{th}_3 - \mathrm{th}_1) \cdot \mathrm{TOT}_2 + \frac{1}{2} \cdot (\mathrm{th}_3 - \mathrm{th}_2) \cdot \mathrm{TOT}_3 \tag{2.2}$$

$$E = \frac{1}{2} \cdot (\mathrm{th}_1 + \mathrm{th}_2) \cdot \mathrm{TOT}_1 + \frac{1}{2} \cdot (\mathrm{th}_3 - \mathrm{th}_1) \cdot \mathrm{TOT}_2 + \frac{1}{2} \cdot (\mathrm{th}_3 - \mathrm{th}_2) \cdot \left(\frac{\mathrm{TOT}_2 \cdot \mathrm{TOT}_3}{\mathrm{TOT}_2 - \mathrm{TOT}_3}\right) \tag{2.3}$$

The performance of the energy estimation using the proposed approach was also compared with that of the conventional single-TOT method. The digital pulse generated by a single comparator before passing through the XOR gate was used for conventional TOT.

2.5 Optimization of pulse shaping and threshold level

We optimized the pulse shaping and threshold level owing to the performance dependence of the proposed methods on these settings. The fast-rising edge of the scintillation pulse can cause timestamps to overlap, resulting in false digital pulses through signal integration using an XOR gate. However, excessive smoothing of the analog pulse with a low-pass filter can degrade the timing performance. Therefore, the employment of minimal low-pass filtering is necessary, which allows for accurate pulse reconstruction. To determine the optimal low-pass filtering conditions, the passive first-order low-pass filters with six different RC constants (5.6 ns, 10 ns, 15 ns, 31.36 ns, 56 ns, and 84 ns) were implemented and tested (figure 2).

We also investigated the effect of threshold level on the energy performance of the proposed method. The lowest threshold level varied between 30 mV and 70 mV in steps of 10 mV. The interval between the three thresholds was also changed from 10 to 40 mV in steps of 10 mV. Average peak height of scintillation pulse was about 400 mV at 84 ns RC constant.

2.6 Event validity check

As mentioned previously, the fast-rising edge of the scintillation pulse can generate false digital pulses through the XOR gate. Therefore, a careful examination of event validity based on prior knowledge of scintillation pulse properties (e.g., the falling edge is longer than the rising edge) is required. Figure 5 shows examples of correct and erroneous digital pulses generated by the XOR

2023 JINST 18 P06021

gate. As shown in figure 5, both four and six timestamps can generate two digital square pulses (A, D, E, and F). Among them, only A can be considered a valid event, because the width of the first pulse occurring on the rising edge is shorter than the width of the second pulse occurring on the falling edge.

Similarly, two and four timestamps can generate a single digital square pulse. Event B in figure 5 can be considered invalid owing to the delay in the first timestamp. Events with more than six timestamps, mainly caused by noisy falling edges, were discarded.

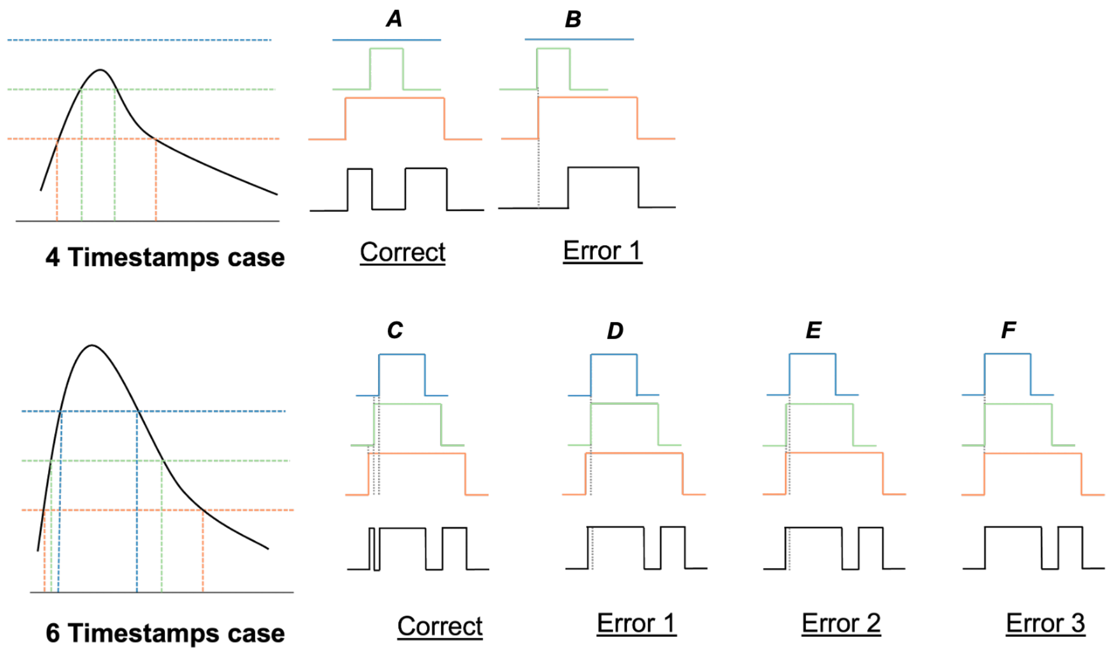

Figure 5. Correct and erroneous digital pulse trains generated by the XOR gate with (a) 4 timestamps and (b) 6 timestamps.

2.7 Energy linearity

The energy linearity of each method was measured using 4 different radiation sources, Co-57, Ba-133, Na-22, Cs-137 with 122 keV, 356 keV, 511 keV and 662 keV, respectively. The true and estimated energy value s were fitted using linear line and the energy linearity was estimated in terms of goodness-of-fit (R^2).

3 Results

3.1 XOR output pulses

Figure 6 shows typical output pulses generated by the XOR gates. A single reference threshold produces two timestamps: one on the rising edge and the other on the falling edge. The numbers of digital pulses and timestamps were determined depending on the magnitude of the scintillation pulse. In all cases, the leading timestamps contain rising edge information, and the trailing timestamps represent falling edge information.

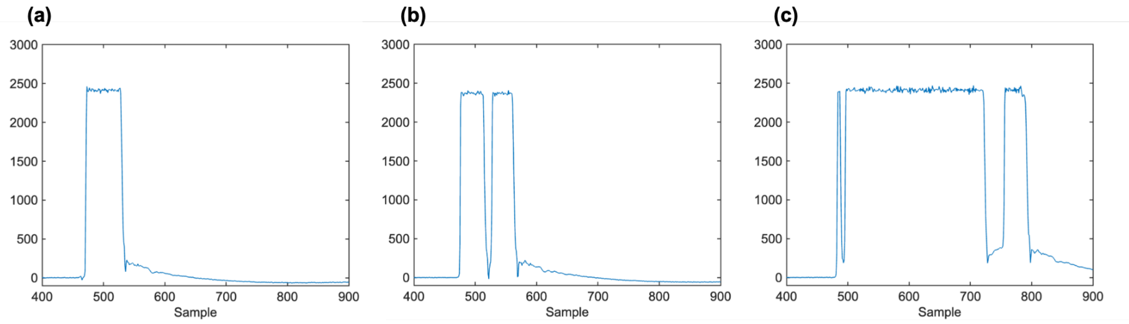

Figure 6. Digital pulse trains recorded using a GHz DRS4 digitizer with (a) 2 timestamps (b) 4 timestamps, and (c) 6 timestamps.

3.2 Event validity

The rate of invalid events was effectively reduced by applying low-pass filters to scintillation pulses. As shown in figure 7, the number of detected errors on the rising and falling edges decreases exponentially as the RC constant of the low-pass filter increases. When a low-pass filter with an 84 ns RC constant was applied, 91% of the detected events showed six timestamps after the event validity check (figure 8). Less than 1% of the events showed more than eight timestamps caused by noise.

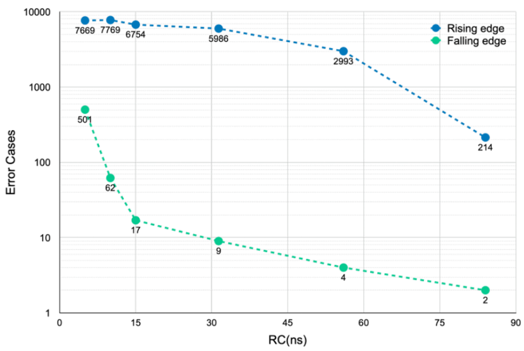

Figure 7. Number of erroneous events out of 10,000 events filtered by event validity check.

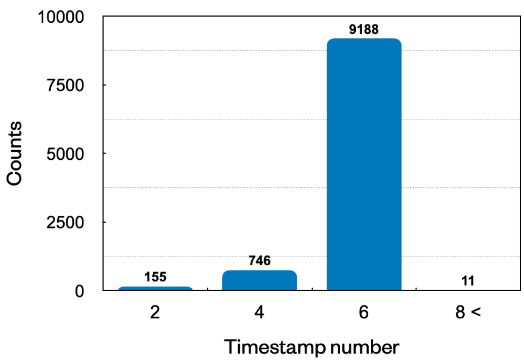

Figure 8. Number of events versus timestamp numbers.

3.3 Energy spectra and resolution

Figure 9 shows the energy spectra measured using the ADC, conventional single TOT, and proposed single-line MVT methods. The spectra were scaled to obtain photopeak positions at 511 keV. For the single-line MVT, an 84 ns RC filter and comparator thresholds of 70, 100, and 130 mV were applied, and the energies were estimated using the *crossing-point triangular sum* method. For a single TOT, a threshold of 70 mV was applied. Low-energy scatter events were not measured by conventional TOT and the proposed single-line MVT methods because of the 70 mV comparator threshold.

2023 JINST 18 P06021

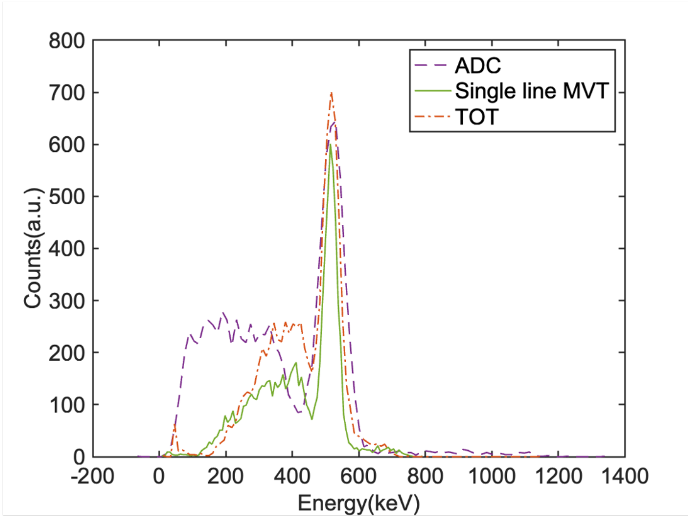

Figure 9. Energy spectra obtained using single-line MVT, simple TOT, and ADC methods.

The energy resolution measured using the single TOT and single-line MVT methods improved with increasing RC constant, as shown in figure 10, where the energy resolution of the single-line MVT is the average of the three different energy estimators. By applying an 84 ns RC filter, we achieved an energy resolution nearly equivalent to that of the ADC (approximately 10%). With this low-pass filter setting, the energy resolution of a single-line MVT improved as the lowest threshold increased when swept at 50, 60, and 70 mV, with the threshold interval fixed at 30 mV (figure 11).

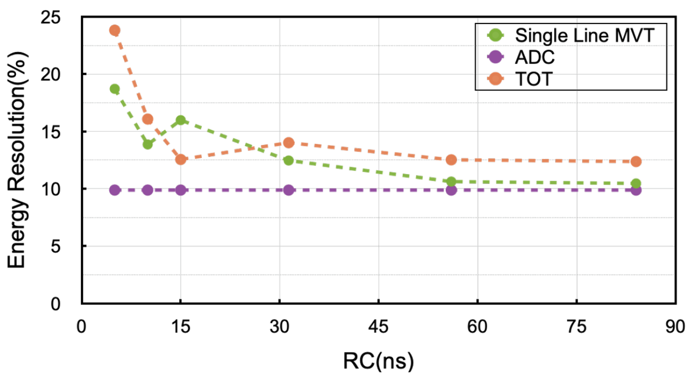

Figure 10. Energy resolution versus RC constants of the low-pass filter.

3.4 Energy linearity

The energy linearity of the proposed method was assessed using events obtained at the optimal setting in terms of energy resolution (84 ns RC filter and 70, 100, and 130 mV thresholds). As shown in figure 12, the proposed single-line MVT outperforms the simple TOT method in terms of goodness-of-fit (R^2). Among the energy estimation methods used in single-line MVT, the *crossing-point triangular sum* method showed the best energy linearity, as 0.96.

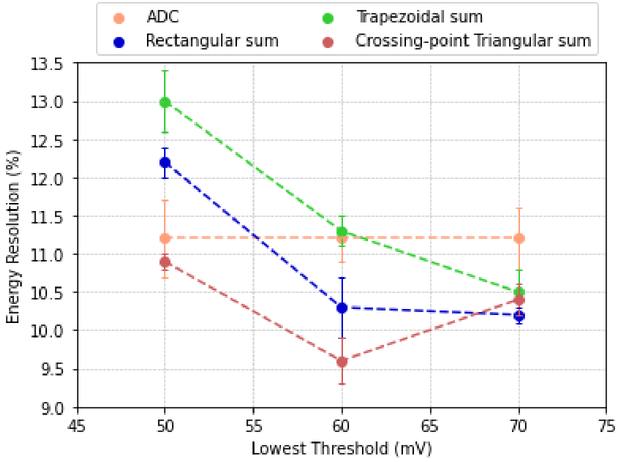

Figure 11. Energy resolution of single-line MVT with different energy estimation (pulse integration) methods ver-sus the lowest threshold.

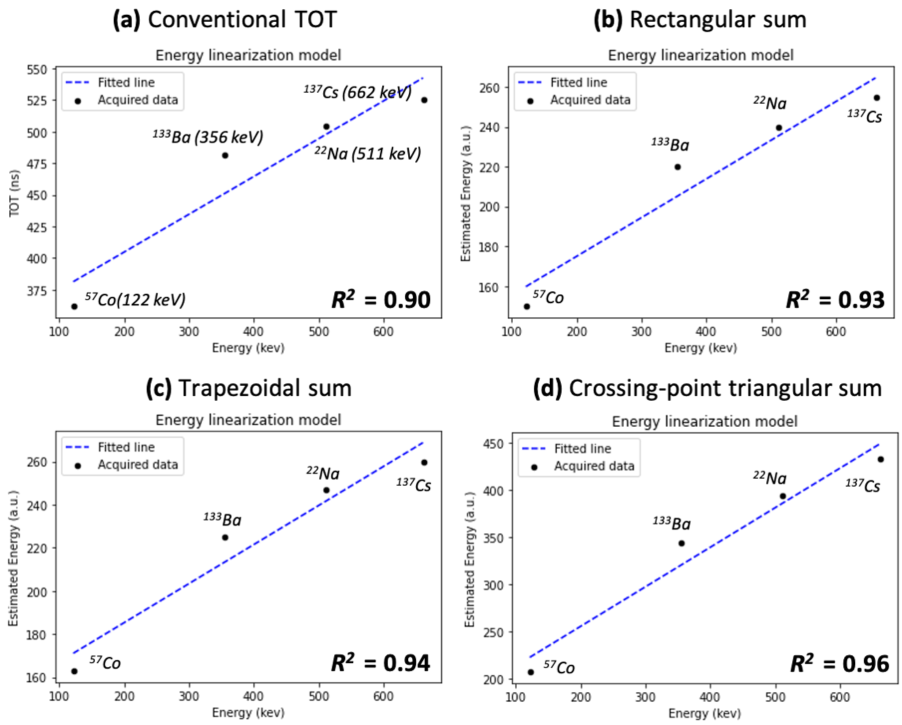

Figure 12. Regression lines indicating a linear relationship between the energy and measurements from 4 different radiation sources on each method.

4 Discussion

The proposed method showed virtually equivalent energy resolution to that of the DRS4-based pulse digitization method and better energy linearity than the conventional TOT method. In conventional TOT, only a pair of sampling points at a fixed threshold is available for energy estimation, leading to

2023 JINST 18 P06021

poor energy resolution and linearity. By contrast, the proposed single-line MVT method collects six sampling points per event; however, it requires only a single digital readout channel. The increased data sampling from an analog pulse allows for a more precise energy estimation as long as proper analog pulse shaping is applied, which is optimized by performing an event validity check.

We compared three different methods (figure 4) for energy estimation using the six sampling points provided by the single-line MVT method. The *crossing-point triangular sum* method showed the best energy resolution and linearity, but its computational complexity was higher than that of other methods. Non-linear curve fitting using specific scintillation pulse modeling may provide better energy estimation performance. However, the substantial computational burden required for nonlinear curve fitting renders real-time energy estimation impossible.

5 Conclusion

In this study, we proposed a single-line MVT method that allows for the reduction of digital output channels from the conventional MVT method by adding an XOR logic gate after the multiple comparators used in the MVT method. The proposed method showed equivalent energy resolution and good energy linearity compared with DRS4-based GHz pulse sampling. This is especially useful when data acquisition systems without ADCs are implemented using FPGA-based TDCs. This is because the proposed method alleviates the problem of limited input ports and the numerous resources required for TDCs in FPGAs.

Acknowledgments

This work was partially supported by the Korea Medical Device Development Fund grant funded by the Korea government (the Ministry of Science and ICT, the Ministry of Trade, Industry and Energy, the Ministry of Health & Welfare, the Ministry of Food and Drug Safety) (Project No. 1711137868 and RS-2020-KD000006).

References

[1] S.I. Kwon et al., *Development of small-animal PET prototype using silicon photomultiplier (SiPM): initial results of phantom and animal imaging studies*, *J. Nucl. Med.* **52** (2011) 572.

[2] E. Roncali and S.R. Cherry, *Application of silicon photomultipliers to positron emission tomography*, *Ann. Biomed. Eng.* **39** (2011) 1358.

[3] S. Gundacker and A. Heering, *The silicon-photomultiplier: fundamentals and applications of a modern solid-state photon detector*, *Phys. Med. Biol.* **65** (2020) 17TR01.

[4] S.J. van der Sar, S.E. Brunner and D.R. Schaart, *Silicon photomultiplier-based scintillation detectors for photon-counting CT: A feasibility study*, *Med. Phys.* **48** (2021) 6324.

[5] G.B. Ko et al., *Simultaneous multiparametric PET/MRI with silicon photomultiplier PET and ultra-high-field MRI for small-animal imaging*, *J. Nucl. Med.* **57** (2016) 1309.

[6] H.S. Yoon et al., *Initial results of simultaneous PET/MRI experiments with an MRI-compatible silicon photomultiplier PET scanner*, *J. Nucl. Med.* **53** (2012) 608.

[7] B. Weissler et al., *A digital preclinical PET/MRI insert and initial results*, *IEEE Trans. Med. Imag.* **34** (2015) 2258.

[8] S. Yamamoto et al., *Simultaneous imaging using SiPM-based PET and MRI for development of an integrated PET/MRI system*, *Phys. Med. Biol.* **57** (2012) N1.

[9] A.M. Grant, B.J. Lee, C.M. Chang and C.S. Levin, *Simultaneous PET/MR imaging with a radio frequency-penetrable PET insert*, *Med. Phys.* **44** (2017) 112.

[10] W. Gsell et al., *Characterization of a preclinical PET insert in a 7 tesla MRI scanner: beyond NEMA testing*, *Phys. Med. Biol.* **65** (2020) 245016.

[11] J.Y. Won et al., *Development and initial results of a brain PET insert for simultaneous 7-Tesla PET/MRI using an FPGA-only signal digitization method*, *IEEE Trans. Med. Imag.* **40** (2021) 1579.

[12] P. Hallen et al., *PET performance evaluation of the small-animal Hyperion II(D) PET/MRI insert based on the NEMA NU-4 standard*, *Biomed. Phys. Eng. Express* **4** (2018) 065027.

[13] J. van Sluis et al., *Performance characteristics of the digital biograph vision PET/CT system*, *J. Nucl. Med.* **60** (2019) 1031.

[14] K.Y. Kim et al., *Performance evaluation of SimPET-X, a PET insert for simultaneous mouse total-body PET/MR imaging*, *Mol. Imaging Biol.* **23** (2021) 703.

[15] A.L. Goertzen et al., *Design and performance of a resistor multiplexing readout circuit for a SiPM detector*, *IEEE Trans. Nucl. Sci.* **60** (2013) 1541.

[16] J. Du et al., *A simple capacitive charge-division readout for position-sensitive solid-state photomultiplier arrays*, *IEEE Trans. Nucl. Sci.* **60** (2013) 3188.

[17] H. Park, G.B. Ko and J.S. Lee, *Hybrid charge division multiplexing method for silicon photomultiplier based PET detectors*, *Phys. Med. Biol.* **62** (2017) 4390.

[18] H. Park, M. Yi and J.S. Lee, *Silicon photomultiplier signal readout and multiplexing techniques for positron emission tomography: a review*, *Biomed. Eng. Lett.* **12** (2022) 263.

[19] H. Kim et al., *A silicon photo-multiplier signal readout using strip-line and waveform sampling for positron emission tomography*, *Nucl. Instrum. Meth. A* **830** (2016) 119.

[20] J.Y. Won, G.B. Ko and J.S. Lee, *Delay grid multiplexing: simple time-based multiplexing and readout method for silicon photomultipliers*, *Phys. Med. Biol.* **61** (2016a) 7113.

[21] J.H. Jung, Y. Choi, J. Jung and S. Kim, *Development of a high-density position decoder circuit for GAPD-based PET with a large number of readout channels*, *Nucl. Instrum. Meth. A* **741** (2014) 117.

[22] S. Lee, Y. Choi, J. Kang and J.H. Jung, *Development of a multiplexed readout with high position resolution for positron emission tomography*, *Nucl. Instrum. Meth. A* **850** (2017) 42.

[23] M. Ito, M.S. Lee and J.S. Lee, *Continuous depth-of-interaction measurement in a single-layer pixelated crystal array using a single-ended readout*, *Phys. Med. Biol.* **58** (2013) 1269.

[24] E. Lamprou, A.J. Gonzalez, F. Sanchez and J.M. Benlloch, *Exploring TOF capabilities of PET detector blocks based on large monolithic crystals and analog SiPMs*, *Phys. Med.* **70** (2020) 10.

[25] H. Li et al., *The Engineering and Initial Results of a Transformable Low-cost High-Resolution PET Camera*, *IEEE Trans. Nucl. Sci.* **54** (2007) 1583.

[26] J.W. Cates and C.S. Levin, *Advances in coincidence time resolution for PET*, *Phys. Med. Biol.* **61** (2016) 2255.

[27] S.I. Kwon, A. Gola, A. Ferri, C. Piemonte and S.R. Cherry, *Bismuth germanate coupled to near ultraviolet silicon photomultipliers for time-of-flight PET*, *Phys. Med. Biol.* **61** (2016) L38.

[28] D.R. Schaart, *LaBr(3):Ce and SiPMs for time-of-flight PET: achieving 100 ps coincidence resolving time*, Phys. Med. Biol. **55** (2010) N179.

[29] J.Y. Yeom, R. Vinke and C.S. Levin, *Optimizing timing performance of silicon photomultiplier-based scintillation detectors*, Phys. Med. Biol. **58** (2013) 1207.

[30] J.W. Son et al., *Proof-of-concept prototype time-of-flight PET system based on high-quantum-efficiency multianode PMTs*, Med. Phys. **44** (2017) 5314.

[31] J.Y. Won et al., *Comparator-less PET data acquisition system using single-ended memory interface input receivers of FPGA*, Phys. Med. Biol. **65** (2020) 155007.

[32] F. Bourgeois, *Proposal for a fast, zero suppressing circuit for the digitization of analog pulses over long memory times*, Nucl. Instrum. Meth. A **219** (1984) 153.

[33] T. Fujiwara, H. Takahashi, K. Shimazoe and B. Shi, *Multi-Level Time-Over-Threshold Method for Energy Resolving Multi-Channel Systems*, IEEE Trans. Nucl. Sci. **57** (2010) 2545.

[34] I. Kipnis et al., *A time-over-threshold machine: The readout integrated circuit for the BaBar silicon vertex tracker*, IEEE Trans. Nucl. Sci. **44** (1997) 289.

[35] T.C. Meyer et al., *A time-based front end readout system for PET & CT*, IEEE Nucl. Sci. Symp. Conf. Rec. **2006** (2006) 2494.

[36] Q. Shen et al., *A 1.7 ps Equivalent Bin Size and 4.2 ps RMS FPGA TDC Based on Multichain Measurements Averaging Method*, IEEE Trans. Nucl. Sci. **62** (2015) 947.

[37] J. Wang, S. Liu, L. Zhao, X. Hu and Q. An, *The 10-ps multitime measurements averaging TDC implemented in an FPGA*, IEEE Trans. Nucl. Sci. **58** (2011) 2011.

[38] J.Y. Won, S.I. Kwon, H.S. Yoon, G.B. Ko, J.W. Son and J.S. Lee, *Dual-phase tapped-delay-line time-to-digital converter with on-the-fly calibration implemented in 40 nm FPGA*, IEEE Trans. Biomed. Circuits Syst. **10** (2016) 231.

[39] J.Y. Won and J.S. Lee, *Time-to-digital converter using a tuned-delay line evaluated in 28-, 40-, and 45-nm FPGAs*, IEEE Trans. Instrum. Meas. **65** (2016) 1678.

[40] J.Y. Yeom, I. Defendi, H. Takahashi, K. Zeitelhack, M. Nakazawa and H. Murayama, *A 12-channel CMOS preamplifier-shaper-discriminator ASIC for APD and gas counters*, IEEE Nucl. Sci. Symp. Conf. Rec. **2005** (2005) 391.

[41] K. Shimazoe et al., *Dynamic time over threshold method*, IEEE Trans. Nucl. Sci. **59** (2012) 3213.

[42] Y. Wang, X. Cheng, D. Li, W. Zhu and C. Liu, *A Linear Time-Over-Threshold Digitizing Scheme and Its 64-channel DAQ Prototype Design on FPGA for a Continuous Crystal PET Detector*, IEEE Trans. Nucl. Sci. **61** (2014) 99.

[43] G.B. Ko and J.S. Lee, *Time-based signal sampling using sawtooth-shaped threshold*, Phys. Med. Biol. **64** (2019) 125020.

[44] H. Kim et al., *A multi-threshold sampling method for TOF PET signal processing*, Nucl. Instrum. Meth. A **602** (2009) 618.

[45] Q. Xie et al., *Initial implementation of LYSO-PSPMT block detector with an all digital DAQ system*, IEEE Nucl. Sci. Symp. Conf. Rec. **2010** (2010) 1759.

[46] H. Wang, J. Liu, H. Zhang, H. Liang and B. Ye, *Multiple time-over-threshold readout electronics for fast timing and energy resolving in a SiPM-based positron annihilation lifetime spectrometer*, 2020 JINST **15** P11006.

[47] K.B. Kim, Y. Choi, J. Jung, S. Lee, H.J. Choe and H.T. Leem, *Analog and digital signal processing method using multi-time-over-threshold and FPGA for PET*, Med. Phys. **45** (2018) 4104.

2023 JINST 18 P06021